Heliyon 9 (2023) e20472

Contents lists available at ScienceDirect

Heliyon

journal homepage: www.cell.com/heliyon

Diagnostic performance of a new two-dimensional shear wave elastography expression using siemens ultrasound system combined with ACR TI-RADS for classification of benign and malignant thyroid nodules: A prospective multi-center study

Wei-Hong Qi [a,1], Kun Jin [a,1], Liu-Liu Cao [a], Mei Peng [a], Nian-An He [b], Xiao-Lin Zhan [c], Yang Yang [b], Yun-Yun Guo [a], Xin-Wu Cui [d], Fan Jiang [a,*]

[a] *Department of Medical Ultrasound, The Second Affiliated Hospital of Anhui Medical University, Hefei, Anhui, 230601, PR China*
[b] *The First Affiliated Hospital of USTC, Division of Life Sciences and Medicine, University of Science and Technology of China, Hefei, Anhui, 230001, PR China*
[c] *Department of Medical Ultrasound, The Fourth Affiliated Hospital of Anhui Medical University, Hefei, Anhui, 230012, PR China*
[d] *Department of Medical Ultrasound, Tongji Hospital of Tongji Medical College, Huazhong University of Science and Technology, Wuhan, Hubei, 430030, PR China*

ARTICLE INFO

Keywords:
Thyroid nodules
Ultrasound
Two-dimensional shear wave elastography
ACR TI-RADS
Pathology

ABSTRACT

Objective: The present study aimed to evaluate the efficacy of a new two-dimensional shear wave elastography (2D-SWE) method using a Siemens ultrasound system and its combination with the American College of Radiology Thyroid Imaging Reporting and Data System (ACR TI-RADS) for the differential diagnosis of benign and malignant thyroid nodules.

Methods: Conventional ultrasound images and 2D-SWE (E-whole-mean and E-stiffest-mean) were prospectively analyzed in 593 thyroid nodules from 543 patients. Nodules were divided into diameter (D) $\leq$10 mm and D $>$ 10 mm groups and graded using ACR TI-RADS. The receiver operating characteristic curve was plotted using pathological findings as the gold standard. Diagnostic performance was compared among 2D-SWE, ACR TI-RADS, and their combination.

Results: The area under the curve (AUC) for E-whole-mean was higher than that for E-stiffest-mean (0.858 vs. 0.790, $P < 0.001$), which indicated that it was the better 2D-SWE parameter for differentiating malignant nodules from benign nodules with an optimal cut-off point of 11.36 kPa. In the all-sizes group, the AUC for E-whole-mean was higher than that for ACR TI-RADS (0.858 vs. 0.808, $P < 0.001$). The combination of E-whole-mean and ACR TI-RADS resulted in a higher AUC (0.929 vs. 0.858 vs. 0.808, $P < 0.001$), sensitivity (87.0% vs. 80.3% vs. 85.2%), specificity (85.1% vs. 74.0% vs. 73.6%), accuracy (86.3% vs. 78.1% vs. 81.1%), positive predictive value (91.5% vs. 85.1% vs. 85.6%), and negative predictive value (78.0% vs. 67.0% vs. 72.9%) compared to E-whole-mean or ACR TI-RADS alone. The AUC for the combination of 2D-SWE and ACR TI-RADS was superior to that for E-whole-mean or ACR TI-RADS alone in both D $\leq$ 10 mm and D $>$ 10 mm groups ($P < 0.001$).

Conclusion: As the better 2D-SWE parameter, E-whole-mean had a higher diagnostic power than ACR TI-RADS and enhanced the diagnostic performance of ACR TI-RADS when identifying benign

* Corresponding author.
E-mail address: ahultrasound2005@126.com (F. Jiang).
[1] These authors contributed equally to this work.

https://doi.org/10.1016/j.heliyon.2023.e20472
Received 15 August 2023; Received in revised form 19 September 2023; Accepted 26 September 2023
Available online 27 September 2023

and malignant thyroid nodules. The combination of E-whole-mean and ACR TI-RADS improved the diagnostic performance compared to using ACR TI-RADS alone, providing a new and reliable method for the clinical diagnosis of thyroid nodules.

1. Introduction

Ultrasound is the first-line and preferred examination method for thyroid nodules [1,2]. Thyroid nodules are increasingly being diagnosed with the development of high-resolution ultrasound [3]. The rate of thyroid nodule detection using ultrasound examination has been reported to range from 20% to 76% [4]. Most of these discovered nodules are benign [5]. Malignant thyroid nodules identified by ultrasound have solid components, irregular margins, micro-calcifications, and taller-than-wide shapes [6,7]. However, ultrasound examination faces challenges in characterizing benign and malignant nodules due to the overlap in some of their features. As a result, no single feature is highly predictive of thyroid malignancy [8].

Ultrasound-guided fine-needle aspiration (FNA) is the gold standard for diagnosing benign and malignant thyroid nodules. However, with the increase in the number of thyroid nodules detected by high-frequency ultrasound, the rate of thyroid nodule FNA has become remarkably high worldwide. This directly causes unnecessary physical harm and psychological trauma to patients and wastes social and medical resources. Several thyroid nodule risk stratification systems worldwide have been used to help to identify the thyroid nodules that require FNA and to further classify their benign or malignant nature. Such risk stratification utilizes the American College of Radiology Thyroid Imaging Reporting and Data System (ACR TI-RADS) [9], the American Thyroid Association system [5], the Korean TI-RADS [10], and French TI-RADS [11]. The ACR TI-RADS was inspired by the 2009 ACR Breast Imaging Reporting and Data System and was finalized in 2017. It classifies each nodule into five categories based on the total score as follows: TR1 (benign), TR2 (not suspicious), TR3 (mildly suspicious), TR4 (moderately suspicious), and TR5 (highly suspicious for malignancy). Nevertheless, approximately 10% of post-FAN samples end up with no diagnostic outcome, and the cytological diagnosis is equivocal in up to 30% of these cases [12,13]. Therefore, professionals worldwide have been searching for better ways to identify benign and malignant thyroid nodules.

Ultrasound elastography is a noteworthy technique that can estimate tissue stiffness and help to distinguish benign nodules from malignant nodules. Strain imaging was first developed in the 1970s and named elastography by Dr. Jonathan Ophir in 1991 [14]. There are two types of ultrasound elastography: strain elastography (SE) and shear wave elastography (SWE) [15,16]. SE does not allow for quantitative assessment of the tissue and is operator-dependent and less reliable. Instead, SWE uses transverse shear waves generated by mechanical vibrational forces. This technique makes it possible to assess tissue stiffness in an approach that is more quantitative, more reproducible, and less operator-dependent [17]. Therefore, two-dimensional shear wave elastography (2D-SWE) has been used to help in the differential diagnosis of thyroid [17], breast [18], and liver [19]. The current studies have shown that different ultrasound systems have different SWE software and optimal cut-off values. The available studies on 2D-SWE in the Siemens ultrasound systems used virtual touch tissue imaging and quantification (VTIQ) expressed in shear wave speed (m/s). To the best of our knowledge, there has been no research that employs the Siemens ultrasound system for 2D-SWE expressed in Young's modulus (kPa), which is different from the previous studies.

Therefore, this prospective study is the first to use the expression of Young's modulus (kPa) in the Siemens ultrasound system, providing a cut-off value that differs from values reported by previous studies in order to evaluate the diagnostic efficacy of 2D-SWE and its combination with ACR TI-RADS for benign and malignant thyroid nodules. This research may provide a new option for diagnosing benign and malignant thyroid nodules using SWE based on 2D ultrasound.

2. Materials and methods

2.1. Patients

The collection of patients' thyroid nodules was organized jointly by four tertiary care hospitals (the highest level in the hospital hierarchy in Mainland China) and was carried out between February 2021 and June 2022. All nodules were divided into groups with diameters (D) of $\leq$10 mm and >10 mm. The inclusion criteria were as follows: 1. one or more thyroid nodules with a cystic component of <50%; 2. clear ultrasound results and 2D-SWE images preserved before FNA or thyroidectomy; 3. clear pathology report, where all nodules treated with FNA were given The Bethesda System of Thyroid Cytopathology Reports (TBSRTC) grade, such that TBSRTC grade II was considered benign and grades V and VI were considered malignant; and 4. signed informed consent form, including for the publication of accompanying images. The exclusion criteria included: 1. inability to cooperate with the procedure; 2. poor-quality ultrasound images for parameter measurement and analysis; 3. nodules without a precise pathological diagnosis after FNA or surgery; and 4. TBSRTC grade I, III, or IV nodules.

2.2. Ultrasound examination

An ACUSON Sequoia color Doppler ultrasound diagnostic system (Siemens, Germany) equipped with 2D-SWE imaging software was used to obtain the expression of Young's modulus (kPa) with a 10L4 linear array probe, frequency of 3–10 MHz, and measurement range set to 0.5–10.0 m/s. All ultrasound examinations, including conventional ultrasound and 2D-SWE, were performed by

radiologists who had more than five years of thyroid ultrasound experience.

A conventional ultrasound examination was performed. When a target thyroid nodule was located, its general features were observed, including the composition, echogenicity, shape, margin, and echogenic foci and size. The TI-RADS score was calculated according to the ACR TI-RADS categories for each nodule based on five features without considering the nodule size. The total number of points determined the ACR TI-RADS nodule grade, ranging from TR1 (benign) to TR5 (highly suspicious of malignancy).

Furthermore, 2D-SWE imaging examinations were conducted. First, the most extensive section of the thyroid nodule was selected to activate 2D-SWE. The operator placed the probe vertically on the skin surface without pressure and then set up the sampling frame, which covered the nodules and the surrounding normal thyroid tissue. After the image quality stabilized, the operator instructed the patient to hold their breath for 2–3 s and then pressed the update button. The circular region of interest (ROI was adjusted to be as close as possible to the size of the nodules to minimize errors. Then, a 3-mm ROI was placed at the same depth as the normal gland. Next, a 3-mm ROI was located at the stiffest part of the nodule and the same depth as the normal gland. The average of three nodule measurements was calculated for more accurate results. In the present report, 2D-SWE of the whole lesion was denoted as E-whole-mean (kPa), and the stiffest elastic part of the lesion was represented as E-stiffest-mean (kPa).

2.3. Statistical analysis

SPSSS 25.0 for Windows (SPSS Institute, USA) and MedCalc 19.0 (MedCalc Software Ltd., Belgium) software packages were used for all statistical analyses. The independent samples T-test was used to quantify continuous variables, such as age, which were expressed as mean ± standard deviation. The chi-square test was used for categorical variables. Non-normality and non-variance homogeneity parameters were described by the median and interquartile range. Wilcoxon and Kruskal-Wallis tests were used to compare whether there were statistical differences in 2D-SWE parameters among the three groups. Parameters of joint indices were obtained using logistic regression. Receiver operating characteristic (ROC) curves were plotted for each group. The area under the curve (AUC), 95% confidence interval (95% CI), cut-off values, sensitivity, specificity, accuracy, positive predictive value (PPV), and negative predictive value (NPV) were also obtained. Finally, the DeLong test in ROC curve analysis was used to compare whether there was a statistical difference between AUCs. For all of the above comparisons, $P < 0.05$ was considered to be statistically significant.

3. Results

3.1. General information

There were 595 patients with 648 thyroid nodules initially included in the study. A total of 55 nodules were excluded based on the exclusion criteria. The final analysis evaluated 593 thyroid nodules in 543 patients (Fig. 1). Among them, there were 392 lesions with maximal $D \leq 10$ mm according to conventional ultrasound measurements. There was a significant difference in age among benign and

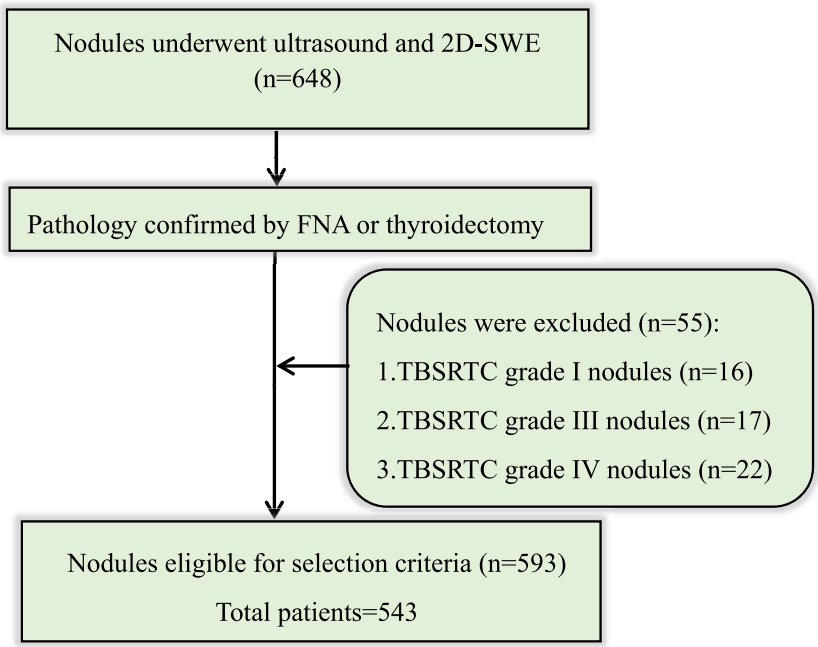

Fig. 1. Flow chart of thyroid nodule selection and exclusion. (2D-SWE = two-dimensional shear wave elastography, FNA = fine needle aspiration cytology, TBSRTC=The Bethesda System for Reporting Thyroid Cytopathology).

malignant nodules in the all-sizes and D > 10 mm groups (P < 0.001), as well as in the sizes of the nodules between benign and malignant nodules in the all-sizes, D ≤ 10 mm, and D > 10 mm groups. There was no significant difference in gender in all three groups (P = 0.372, 0.898, and 0.284, respectively) (Table 1).

3.2. Pathological and ACR TI-RADS classification

Among the 593 thyroid nodules, 208 were benign and 385 were malignant. FNA confirmed that 151 of 208 benign nodules had no specific pathological type, and the remaining benign nodules were confirmed by postoperative pathology to be predominantly nodular goiter and Hashimoto's thyroiditis (HT). All malignant thyroid nodules were confirmed by postoperative pathology, and the pathological types were all papillary thyroid carcinoma (PTC). The pathological findings are summarized in Table 2.

Based on the ROC curve, TR5 was selected as the optimal cut-off value for diagnosing benign and malignant nodules by ACR TI-RADS. General distribution of the ACR TI-RADS classification according to pathological findings is summarized in Table 3.

3.3. 2D-SWE findings

In the all-sizes, D ≤ 10 mm, and D > 10 mm groups, 2D-SWE parameters in malignant nodules were higher than those in benign nodules as demonstrated by E-whole-mean (16.10 kPa vs. 7.90 kPa, 15.90 kPa vs. 8.00 kPa, and 17.30 kPa vs. 7.9 kPa, respectively) and E-stiffest-mean (22.20 kPa vs. 13.9 kPa, 20.70 kPa vs. 10.45 kPa, and 17.30 kPa vs. 7.9 kPa, respectively). E-whole-mean and E-stiffest-mean were higher than those in the normal glands at the same depth. These comparisons were statistically significant (P < 0.001; Table 4). Examples of benign nodules (Fig. 2A–D) and malignant (Fig. 3A–D) nodules are shown separately and include conventional ultrasound and 2D-SWE results.

In the all-sizes group, E-whole-mean had a better diagnostic performance than E-stiffest-mean based on the values for AUC (0.858 vs. 0.79, P = 0.001), sensitivity (80.3% vs. 75.1%), specificity (74.0% vs. 68.3%), accuracy (78.1% vs. 72.7%), PPV (85.1% vs. 81.4%), and NPV (67.0% vs. 59.7%) (Fig. 4A). The AUC for E-whole-mean was higher than that of E-stiffest-mean in the D ≤ 10 mm (0.868 vs. 0.866) (Fig. 4B) and D > 10 mm (0.856 vs. 0.812) groups (Fig. 4C), although these results were not statistically significant (P = 0.886, 0.070, respectively). In these three groups, the optimal cut-off values for E-whole-mean were 11.35 kPa, 12.55 kPa, and 9.85 kPa, respectively (Table 5).

3.4. Diagnostic performance of E-whole-mean in combination with ACR TI-RADS

In the all-sizes group, the AUC for E-whole-mean was higher than that of ACR TI-RADS (0.858 vs. 0.808, P < 0.001), with comparable specificity, accuracy, PPV, and NPV. The AUC for the combination of E-whole-mean and ACR TI-RADS was significantly higher than that of E-whole-mean or ACR TI-RADS alone (0.929 vs. 0.858 vs. 0.808), with statistical significance determined using the two-by-two comparisons (all P values < 0.05; Tables 6 and 7). The combination of E-whole-mean and ACR TI-RADS had superior sensitivity, specificity, accuracy, PPV, and NPV than E-whole-mean or ACR TI-RADS alone (Table 6, Fig. 5A).

In the D ≤ 10 mm group, the AUC for E-whole-mean was higher than that for ACR TI-RADS (0.868 vs. 0.746, P < 0.001), with a higher specificity and PPV. The AUC for the combination of E-whole-mean and ACR TI-RADS was significantly higher than that for E-whole-mean or ACR TI-RADS alone (0.920 vs. 0.868 vs. 0.746), with a statistical significance in the two-by-two comparisons (all P values < 0.001; Tables 6 and 7). The combination of E-whole-mean and ACR TI-RADS had superior sensitivity, specificity, accuracy, PPV, and NPV than ACR TI-RADS alone (Table 6, Fig. 5B).

In the D > 10 mm group, the AUC for E-whole-mean was slightly lower than that for ACR TI-RADS (0.856 vs. 0.858), but this result

Table 1
Summary of patients' general information.

Parameter	Benign	Malignant	Total	*P-value*
Total	208	385	593	
Age (y)	47.59 ± 11.33	43.55 ± 12.25	44.96 ± 12.08	<0.001
Gender				0.372
Female	165 (79.3%)	293 (76.1%)	458 (77.2%)	
Male	43 (20.7%)	92 (23.9%)	135 (22.8%)	
Mean nodule size (mm)	13.27 ± 9.18	8.23 ± 5.13	11.23 ± 7.23	<0.001
D ≤ 10 mm	100	292	392 (66.1%)	
Age	46.51 ± 12.74	43.81 ± 11.55	44.50 ± 11.91	0.050
Gender				0.898
Female	77 (77.0%)	223 (76.4%)	300 (76.5%)	
Male	23 (23.0%)	69 (23.6%)	92 (23.5%)	
Mean nodule size (mm)	6.46 ± 2.02	5.99 ± 2.01	6.11 ± 2.03	<0.001
D > 10 mm	103	98	201 (33.9%)	
Age	48.58 ± 9.79	42.73 ± 14.26	45.88 ± 12.38	0.001
Gender				0.284
Female	88 (81.5%)	70 (75.3%)	158 (78.6%)	
Male	20 (18.5%)	23 (24.7%)	43 (21.4%)	
Mean nodule size (mm)	19.57 ± 8.70	15.23 ± 5.63	17.57 ± 7.73	<0.001

Table 2
Pathological distribution of 593 thyroid nodules.

Pathology results	Specific pathological typing	n
Benign (n = 208)		
FNA	No specific pathological typing	151
Thyroidectomy	Nodular goiter	28
	Hashimoto's thyroiditis (HT)	24
	Subacute thyroiditis	4
	Granulomatous inflammation	1
Malignant (n = 385)		
FNA	Papillary thyroid carcinoma (PTC)	176
Thyroidectomy	Papillary thyroid carcinoma (PTC)	209
Total		593

FNA = fine-needle aspiration.

Table 3
Distribution of ACR TI-RADS categories according to pathology results.

		Pathologic diagnosis		Total	Malignancy rate (%)	*P-value*
		Malignant(n)	Benign (n)			
						<0.001
ACR TI-RADS	TR2	0	13	13	0	
	TR3	1	30	31	3	
	TR4	56	110	166	33	
	TR5	328	55	383	85	
	Total	385	208	593	64	

Table 4
2D-SWE results for 593 thyroid nodules.

	Benign (kPa)	Malignant (kPa)	*P-value*
Total			
E-whole-mean	7.90 (5.50–11.70)	16.10 (12.20–24.50)	<0.001
Glands of equal depth	7.40 (5.10–10.45)	13.70 (9.40–19.70)	<0.001
E-stiffest-mean	13.90 (8.90–18.40)	22.20 (16.60–32.10)	<0.001
Glands of equal depth	7.60 (5.10–11.90)	14.30 (9.60–20.30)	<0.001
D ≤ 10 mm			
E-whole-mean	8.00 (5.50–11.35)	15.90 (12.40–22.60)	<0.001
Glands of equal depth	7.15 (4.80–9.75)	13.70 (9.80–19.45)	<0.001
E-stiffest-mean	10.45 (7.70–15.00)	20.70 (15.70–29.10)	<0.001
Glands of equal depth	6.80 (4.70–10.25)	13.90 (9.60–19.60)	<0.001
D > 10 mm			
E-whole-mean	7.90 (5.35–2.45)	17.30 (11.50–30.70)	<0.001
Glands of equal depth	7.75 (5.30–11.30)	12.90 (8.80–21.20)	<0.001
E-stiffest-mean	16.10 (12.20–21.00)	31.10 (19.40–44.70)	<0.001
Glands of equal depth	8.30 (5.65–12.65)	15.10 (9.60–21.50)	<0.001

2D-SWE = two-dimensional shear wave elastography.

was not statistically significant (P = 0.955). The AUC for the combination of E-whole-mean and ACR TI-RADS was higher than that for E-whole-mean or ACR TI-RADS alone (0.935 vs. 0.858 vs. 0.856), while the two-by-two comparison results did not identify any statistical significance in this result (Tables 6 and 7). The combination of E-whole-mean and ACR TI-RADS had superior sensitivity, specificity, accuracy, PPV, and NPV than ACR TI-RADS alone (Table 6, Fig. 5C).

4. Discussion

A new 2D-SWE expression using Young's modulus (in kPa) obtained using a Siemens ultrasound system was employed in the present study. This investigation aimed to evaluate the diagnostic efficacy of 2D-SWE parameters (E-whole-mean, E-stiffest-mean) and combined the better parameter with ACR TI-RADS to distinguish benign and malignant thyroid nodules. The comparison showed that E-whole-mean was superior to E-stiffest-mean and enhanced the diagnostic performance of ACR TI-RADS when identifying benign and malignant nodules. This suggested that 2D-SWE could be an adjunct to conventional ultrasound imaging to help identify benign and malignant thyroid nodules more effectively.

The present study adopted E-whole-mean and E-stiffest-mean from 2D-SWE to assess the stiffness of thyroid nodules. In all three groups, E-whole-mean and E-stiffest-mean values for malignant nodules were higher than those for benign nodules. Although the

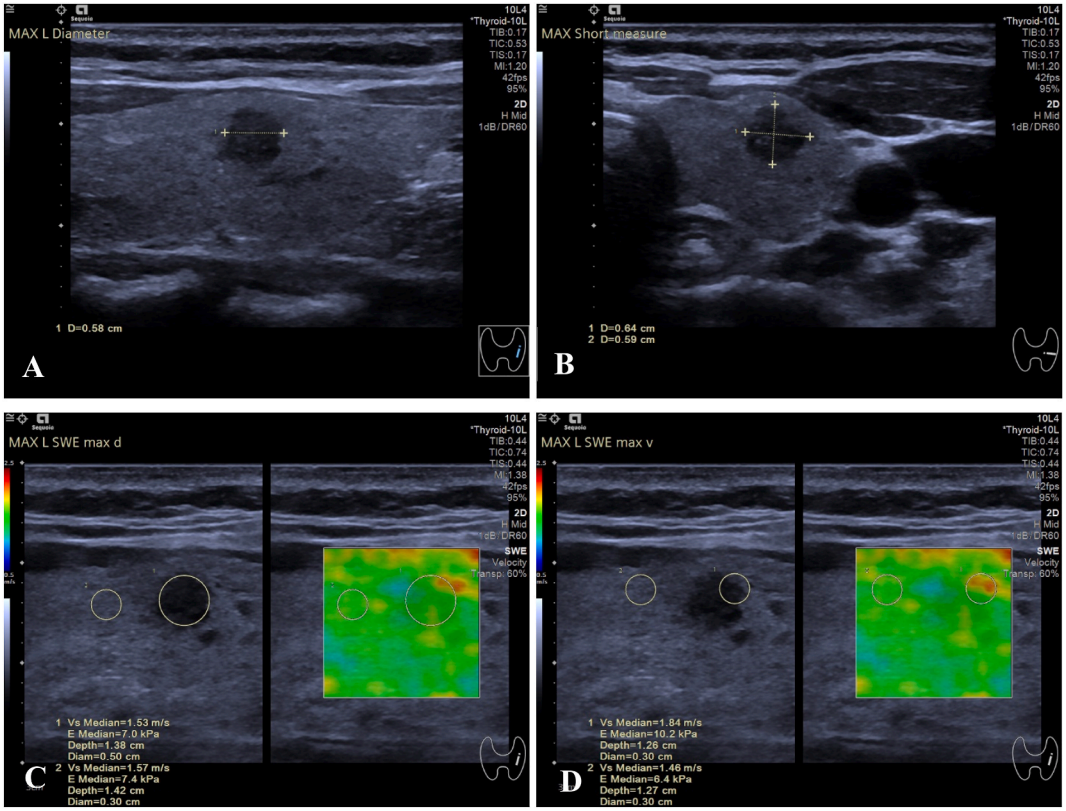

Fig. 2. Surgery-proven nodular goiter with size 5.8 × 6.4 × 5.9 mm in a 45-year-old woman. (A, B) Long- and short-axis views of thyroid nodule in 2D ultrasound. The nodule had a less clear border and relatively regular morphology. (C) E-whole-mean is 7.0 kPa, and that of the normal gland at roughly the same depth is 7.4 kPa. (D) E-stiffest-mean is 10.2 kPa, and that of the normal gland at roughly the same depth is 6.4 kPa.

selected SWE parameters were different, some studies have come to conclusions that were consistent with that of the present study [20,21]. The present research demonstrated that 2D-SWE is a feasible technique to identify malignancy, providing quantitative tissue stiffness information consistent with that described by previous studies [20,22,23]. The pathological features of thyroid nodules pointed to a softer texture in benign nodules and a harder texture in malignant nodules. PTC has a more complex texture because it has sandy, granular components and tends to be extensively fibrotic. In contrast, benign thyroid nodules mainly comprise follicular structures filled with gelatin and therefore have a softer texture [24,25]. Thus, 2D-SWE can be used as an "electronic palpation" method to help determine the nature of the nodules. With a higher AUC, sensitivity, specificity, accuracy, PPV, and NPV compared to E-stiffest-mean in all three groups (except for the slightly higher sensitivity and accuracy in the D $\leq$ 10 mm group), E-whole-mean was chosen in combination with ACR TI-RADS for further study. The effective identification of benign and malignant nodules suggested that 2D-SWE is an important addition to conventional ultrasound in the characterization of thyroid nodules, and it might be valuable to introduce 2D-SWE into routine clinical practice.

Previous studies have shown that different ultrasound systems have different optimal parameters and cut-off values for SWE to differentiate benign and malignant thyroid nodules. A meta-analysis showed that different ultrasound instruments and software provided different optimal parameters and cut-off values. SWE using a Supersonics ultrasound system was expressed in kilopascals, and VTIQ using a Siemens ultrasound system provided quantitative data in meters per second. Both metrics (meters per second and kilopascals) were available from a Toshiba ultrasound system [26]. The present study provided a new SWE modality of 2D-SWE expressed via Young's modulus using a Siemens ultrasound system, with the optimal cut-off values of E-whole-mean of 11.35 kPa and E-stiffest-mean of 16.50 kPa in the all-sizes group. This method represents an additional option for clinical assistance in diagnosing benign and malignant thyroid nodules. The differences in SWE parameters and cut-off values can be attributed to the differences in each device's acquisition, ROI size, and location characteristics.

The present study set TR5 as the cut-off value for benign and malignant nodules using the maximum Jorden index. The malignancy risk incidence values calculated for TR4 using ACR TI-RADS were higher (33%) than those provided by the guidelines (5–20%), which may be related to the fact that 66.1% of the nodules analyzed in the study were microscopic. Due to the small size of the nodules resulting in malignant signs not being well expressed on 2D ultrasound, some of the malignant nodules corresponded to a lower risk stratification classification. In a meta-analysis of ACR TI-RADS involving 1001 thyroid nodules, the pooled sensitivity and specificity were 61% and 88%, respectively [27]. The present study showed a higher sensitivity (80.3%) and slightly lower specificity (74.0%) than the meta-analysis. The lower specificity indicated that some nodules were misdiagnosed and overtreated. Therefore, new methods

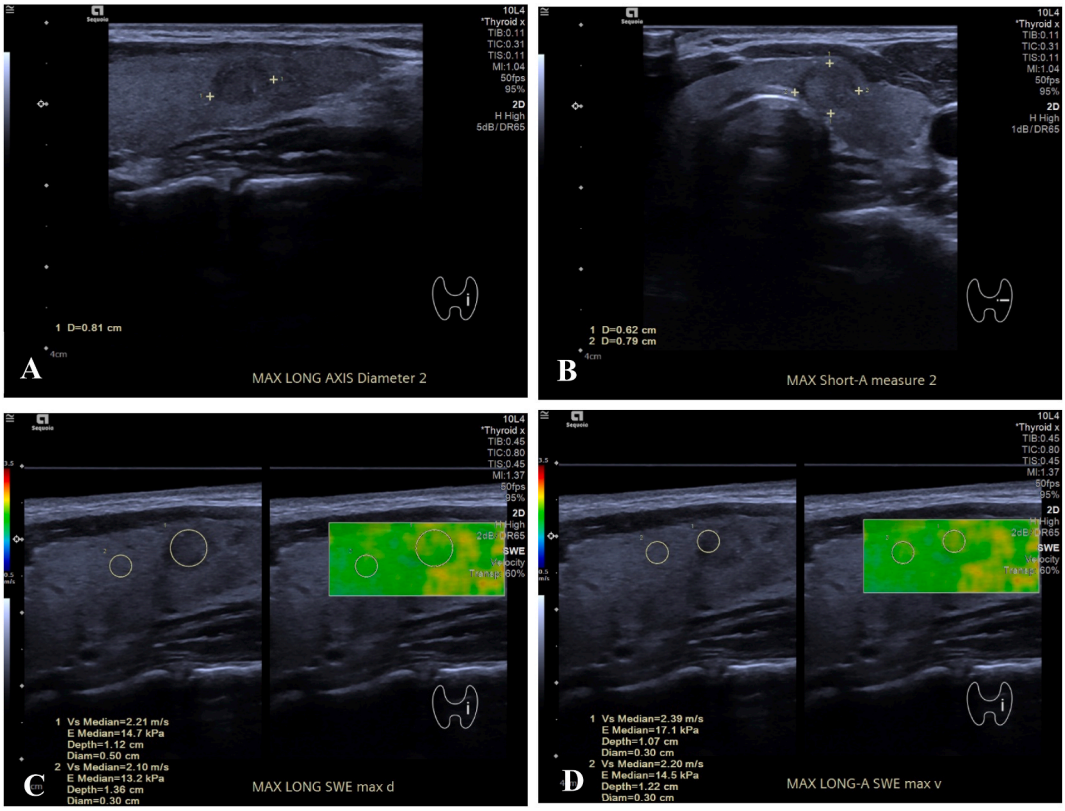

Fig. 3. Surgery-proven papillary thyroid microcarcinoma (PTMC) with size 8.1 × 6.2 × 7.9 mm in a 35-year-old woman. (A, B) Long- and short-axis views of thyroid nodule in 2D ultrasound. The nodule had a relatively clear boundary and regular morphology. (C) E-whole-mean is 14.7 kPa, and that of the normal gland at roughly the same depth is 13.2 kPa. (D) E-stiffest-mean is 17.1 kPa, and that of the normal gland at roughly the same depth is 14.5 kPa.

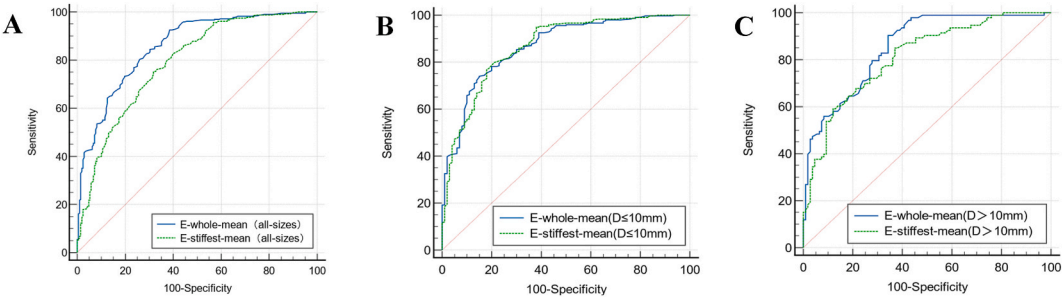

Fig. 4. Receiver operating characteristic (ROC) curves for E-whole-mean and E-stiffest-mean. (A) Area under the curve (AUC) for E-whole-mean and E-stiffest-mean was 0.858 and 0.790, respectively, in all-sizes group. (B) AUC for E-whole-mean and E-stiffest-mean was 0.868 and 0.866, respectively, in D ≤ 10 mm group. (C) AUC for E-whole-mean and E-stiffest-mean was 0.856 and 0.812, respectively, in D > 10 mm group.

are needed to improve diagnostic efficiency for thyroid nodules to avoid unnecessary FNA and surgery, thus reducing undue patient discomfort.

The present study concluded that combining E-whole-mean and ACR TI-RADS significantly improved AUC, sensitivity, specificity, accuracy, PPV, and NPV for diagnosing benign and malignant nodules compared to both of the methods alone in the all-sizes group, which was in accordance with the reports by Makal et al. and He et al. [28,29]. When comparing SWE and ACR TI-RADS classification, the present study showed that E-whole-mean based on SWE parameters demonstrated a better diagnostic AUC than ACR TI-RADS in the all-sizes group when diagnosing benign and malignant nodules, which was similar to the results from a study by Makal et al. [28]. However, the diagnostic sensitivity of E-whole-mean (80.3%) in the present study was slightly lower than that of the ACR TI-RADS classification (85.2%), which was compensated by the combined diagnosis using both methods (87.0%). In summary, the present study suggested that the new combination approach significantly improved the detection accuracy of benign and malignant thyroid

Table 5
Diagnostic efficacy of 2D-SWE.

	AUC (95%CI)	Cut-off value(kPa)	Sensitivity (%)	Specificity (%)	Accuracy (%)	PPV (%)	NPV (%)	*P-value of AUC*
Total								0.001
E-whole-mean	0.858 (0.827–0.889)	11.35	80.3	74.0	78.1	85.1	67.0	
E-stiffest-mean	0.790 (0.751–0.829)	16.50	75.1	68.3	72.7	81.4	59.7	
D ≤ 10 mm								0.886
E-whole-mean	0.868 (0.828–0.908)	12.55	74.0	85.0	76.8	93.5	52.8	
E-stiffest-mean	0.866 (0.824–0.908)	15.15	79.8	79.0	79.6	91.7	57.2	
D > 10 mm								0.070
E-whole-mean	0.856 (0.805–0.906)	9.85	90.3	65.7	77.1	69.4	88.7	
E-stiffest-mean	0.812 (0.753–0.870)	18.10	84.9	63.0	73.1	66.4	82.9	

2D-SWE = two-dimensional shear wave elastography; CI = confidence interval; PPV = positive predictive value; NPV = negative predictive value.

Table 6
Diagnostic efficacy of ACR TI-RADS, E-whole-mean, and their combination in thyroid nodules.

	AUC (95%CI)	Cut-off value (kPa)	Sensitivity (%)	Specificity (%)	Accuracy (%)	PPV (%)	NPV (%)	*P-value of AUC*
Total								
ACR TI-RADS	0.808 (0.774–0.843)	5	85.2	73.6	81.1	85.6	72.9	<0.001
E-whole-mean	0.858 (0.827–0.889)	11.35	80.3	74.0	78.1	85.1	67.0	<0.001
Combination of ACR TI-RADS and E-whole-mean	0.929 (0.907–0.950)	0.666	87.0	85.1	86.3	91.5	78.0	<0.001
D ≤ 10 mm								
ACR TI-RADS	0.746 (0.694–0.798)	5	86.6	62.0	80.4	86.9	61.4	<0.001
E-whole-mean	0.868 (0.828–0.908)	12.55	74.0	85.0	76.8	93.5	52.8	<0.001
Combination of ACR TI-RADS and E-whole-mean	0.920 (0.891–0.949)	0.683	88.7	79.0	86.2	92.5	70.5	0.001
D > 10 mm								
ACR TI-RADS	0.858 (0.811–0.904)	5	80.6	84.3	82.6	81.5	83.5	<0.001
E-whole-mean	0.856 (0.805–0.906)	9.85	90.3	65.7	77.1	69.4	88.7	<0.001
Combination of ACR TI-RADS and E-whole-mean	0.935 (0.904–0.967)	0.613	83.9	90.7	87.6	88.6	86.7	<0.001

AUC = area under the curve; CI = confidence interval; PPV = positive predictive value; NPE = negative predictive value.

Table 7
Pair-wise comparison of AUC among ACR TI-RADS, E-whole-mean, and their combination.

	95%CI	z-statistic	*P-value*
Total			
Combination ~ ACR TI-RADS	0.093–0.148	8.476	0.040
Combination ~ E-whole-mean	0.045–0.096	5.376	<0.001
ACR TI-RADS ~ E-whole-mean	0.002–0.011	2.061	<0.001
D ≤ 10 mm			
Combination ~ ACR TI-RADS	0.129–0.219	7.541	<0.001
Combination ~ E-whole-mean	0.022–0.082	3.402	<0.001
ACR TI-RADS ~ E-whole-mean	0.053–0.190	3.490	<0.001
D > 10 mm			
Combination ~ ACR TI-RADS	0.045–0.111	4.630	<0.001
Combination ~ E-whole-mean	0.038–0.121	3.739	<0.001
ACR TI-RADS ~ E-whole-mean	−0.064–0.068	0.0557	0.955

AUC = area under the curve; CI = confidence interval.

nodules, thereby reducing the rate of unnecessary FNA or surgical thyroidectomy. This demonstrated the usefulness of SWE in helping to differentially diagnose benign and malignant thyroid nodules based on 2D ultrasound imaging.

There have been relatively few studies that stratified nodule sizes. Although FNA screening or surgical resection of nodules with D ≤ 10 mm is not recommended in the ACT TI-RADS, microscopic thyroid cancer is not always a low-risk tumor. Approximately 20% of microscopic multifocal cancers will present with metastasis to the lymph nodes in the neck and a higher risk of distant metastasis [21]. This served as the motivation for the present study to investigate the diagnostic efficacy of SWE combined with ACR TI-RADS using D

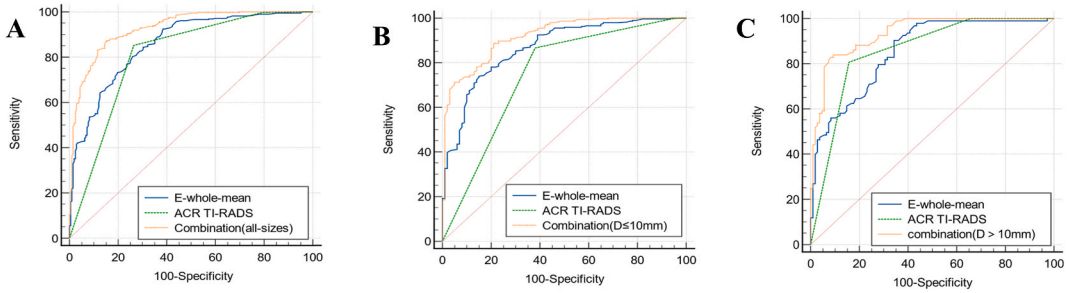

Fig. 5. Receiver operating characteristic (ROC) curves for E-whole-mean alone, ACR TI-RADS alone, and their combination. (A) Area under the curve (AUC) for the combination, E-whole-mean, and ACR TI-RADS was 0.929, 0.858, and 0.808, respectively, in all-sizes group. (B) AUC for the combination, E-whole-mean, and ACR TI-RADS was 0.920, 0.868, and 0.746, respectively, in D $\leq$ 10 mm group. (C) AUC for the combination, E-whole-mean, and ACR TI-RADS was 0.935, 0.858, and 0.856, respectively, in D $>$ 10 mm group.

$\leq$ 10 mm as the nodal size stratification. As shown in the present study, the combination of E-whole-mean and ACR TI-RADS still demonstrated good diagnostic results compared to each of them individually in the D $\leq$ 10 mm and D $>$ 10 mm groups, which was similar to a previous study by Liu Y et al. that evaluated 586 thyroid nodules [30]. In the present study, ACR TI-RADS performed better in the D $>$ 10 mm group, as evidenced by elevated AUC, sensitivity, accuracy, and PPV. The poor performance of ACR TI-RADS grading in nodules with D $\leq$ 10 mm might be caused by the ultrasonographic features of small nodules, such as echogenicity, composition, and presence of calcified foci, which are often poorly represented and challenging to determine, thus making accurate ACR TI-RADS grading more difficult. In contrast, a possible reason for the better performance of the E-whole-mean in the D $\leq$ 10 mm group was that the included malignant nodules were all PTC, which has a more complex texture and more pronounced differences from the surrounding tissue. A similar study by Liu et al. [31] did not show satisfactory diagnostic efficacy in microscopic thyroid nodules. The present study showed that 2D-SWE assesses the nodule stiffness while ACR TI-RADS provides morphological features of nodules. Therefore, 2D-SWE and ACR TI-RADS are complementary in the stratified diagnosis of thyroid nodules. Among them, 2D-SWE has a more obvious advantage in identifying benign and malignant microscopic thyroid nodules on the basis of 2D ultrasound. On the other hand, it facilitates the early detection of potentially malignant microscopic nodules in patients so that appropriate interventions, such as close follow-up, can be undertaken in a timely manner to avoid more serious consequences.

In addition, the present study revealed that patients with malignant thyroid nodules were younger than those with benign nodules. A similar result has also been reported by Sohn et al. [20]. Therefore, a more careful evaluation is needed if a patient is younger when evaluating an uncertain thyroid nodule.

There were some limitations in the present study. First, PTC was the pathological type of all malignancies analyzed, which means that the study did not evaluate non-papillary carcinoma types, such as follicular and undifferentiated carcinomas. Further studies on the differences between non-papillary thyroid carcinoma and PTC in terms of 2D-SWE parameters are needed to obtain SWE parameters for different thyroid carcinomas if a sufficient sample size is available. Second, the present study did not determine whether thyroid nodules were present in coexisting lesions, such as HT. The differences in 2D-SWE parameters between thyroid nodules with and without lesion background will be investigated in the future. Third, a round ROI can lead to some normal thyroid tissue being included in acquiring 2D-SWE for thyroid nodules that are not round in shape, thus reducing the overall 2D-SWE of the lesion. In addition, some information from the envelope or muscular tissue may interfere with thyroid nodules close to the margins. Both of these were tests of 2D-SWE reproducibility. However, 2D-SWE still has good reproducibility as long as pre-compression is reduced and the ROI size and location are checked to avoid obvious gross calcifications or cystic areas.

In conclusion, conventional ultrasound is the basis for diagnosing thyroid nodules. 2D-SWE expressed using Young's modulus obtained using a Siemens ultrasound system provided a different cut-off value compared to previous studies. As a better 2D-SWE parameter, E-whole-mean demonstrated a higher diagnostic efficacy than ACR TI-RADS and enhanced the diagnostic effectiveness of ACR TI-RADS for benign and malignant thyroid nodules. Their combination may provide a novel and reliable method for clinical diagnosis of thyroid nodules.

Author contribution statement

Wei-Hong Qi: Performed the experiments; Analyzed and interpreted the data; Wrote the paper. Kun Jin: Performed the experiments; Analyzed and interpreted the data. Liu-Liu Cao, Mei Peng, Nian-An He, Xiao-Lin Zhan, Yang, Yun-Yun Guo:Performed the experiments.

Data availability statement

Data will be made available on request.

CRediT authorship contribution statement

Wei-Hong Qi: Writing – original draft. **Kun Jin:** Datacuration. **Liu-Liu Cao:** Investigation. **Mei Peng:** Data curation. **Nian-An He:** Data curation. **Xiao-Lin Zhan:** Data curation. **Yang Yang:** Data curation. **Yun-Yun Guo:** Data curation. **Xin-Wu Cui:** Writing – review & editing. **Fan Jiang:** Writing – review & editing.

Declaration of competing interest

The authors declare that they have no known competing financial interests or personal relationships that could have appeared to influence the work reported in this paper.

Appendix A. Supplementary data

Supplementary data to this article can be found online at https://doi.org/10.1016/j.heliyon.2023.e20472.

References

[1] H.J. Moon, J.M. Sung, E.-K. Kim, J.H. Yoon, J.H. Youk, J.Y. Kwak, Diagnostic performance of gray-scale US and elastography in solid thyroid nodules, Radiology 262 (2012) 1002–1013, https://doi.org/10.1148/radiol.11110839.

[2] M.C. Frates, C.B. Benson, J.W. Charboneau, E.S. Cibas, O.H. Clark, B.G. Coleman, J.J. Cronan, P.M. Doubilet, D.B. Evans, J.R. Goellner, I.D. Hay, B.S. Hertzberg, C.M. Intenzo, R.B. Jeffrey, J.E. Langer, P.R. Larsen, S.J. Mandel, W.D. Middleton, C.C. Reading, S.I. Sherman, F.N. Tessler, Management of thyroid nodules detected at US: society of radiologists in ultrasound consensus conference statement, Radiology 237 (2005) 794–800, https://doi.org/10.1148/radiol.2373050220.

[3] G. Ferraioli, R.G. Barr, A. Farrokh, M. Radzina, X.W. Cui, Y. Dong, L. Rocher, V. Cantisani, E. Polito, M. D'Onofrio, D. Roccarina, Y. Yamashita, M.K. Dighe, C. F. Dietrich, How to perform shear wave elastography. Part I, Med. Ultrason. 24 (2022) 95, https://doi.org/10.11152/mu-3217.

[4] B. Wang, X. Ou, J. Yang, H. Zhang, X.-W. Cui, C.F. Dietrich, A.-J. Yi, Contrast-enhanced ultrasound and shear wave elastography in the diagnosis of ACR TI-RADS 4 and 5 category thyroid nodules coexisting with Hashimoto's thyroiditis, Front. Oncol. 12 (2023), 1022305, https://doi.org/10.3389/fonc.2022.1022305.

[5] B.R. Haugen, E.K. Alexander, K.C. Bible, G.M. Doherty, S.J. Mandel, Y.E. Nikiforov, F. Pacini, G.W. Randolph, A.M. Sawka, M. Schlumberger, K.G. Schuff, S. I. Sherman, J.A. Sosa, D.L. Steward, R.M. Tuttle, L. Wartofsky, American thyroid association management guidelines for adult patients with thyroid nodules and differentiated thyroid cancer: the American thyroid association guidelines task force on thyroid nodules and differentiated thyroid cancer, Thyroid 26 (2015) 1–133, https://doi.org/10.1089/thy.2015.0020, 2016.

[6] E.J. Ha, W.-J. Moon, D.G. Na, Y.H. Lee, N. Choi, S.J. Kim, J.K. Kim, A multicenter prospective validation study for the Korean thyroid imaging reporting and data system in patients with thyroid nodules, Korean J. Radiol. 17 (2016) 811, https://doi.org/10.3348/kjr.2016.17.5.811.

[7] E.-K. Kim, C.S. Park, W.Y. Chung, K.K. Oh, D.I. Kim, J.T. Lee, H.S. Yoo, New sonographic criteria for recommending fine-needle aspiration biopsy of nonpalpable solid nodules of the thyroid, Am. J. Roentgenol. 178 (2002) 687–691, https://doi.org/10.2214/ajr.178.3.1780687.

[8] J.K. Hoang, W.K. Lee, M. Lee, D. Johnson, S. Farrell, US features of thyroid malignancy: pearls and pitfalls, Radiographics 27 (2007) 847–860, https://doi.org/10.1148/rg.273065038.

[9] F.N. Tessler, W.D. Middleton, E.G. Grant, J.K. Hoang, L.L. Berland, S.A. Teefey, J.J. Cronan, M.D. Beland, T.S. Desser, M.C. Frates, L.W. Hammers, U.M. Hamper, J.E. Langer, C.C. Reading, L.M. Scoutt, A.T. Stavros, ACR thyroid imaging, reporting and data system (TI-RADS): white paper of the ACR TI-RADS committee, J. Am. Coll. Radiol. 14 (2017) 587–595, https://doi.org/10.1016/j.jacr.2017.01.046.

[10] W.D. Middleton, S.A. Teefey, C.C. Reading, J.E. Langer, M.D. Beland, M.M. Szabunio, T.S. Desser, Comparison of performance characteristics of American College of Radiology TI-RADS, Korean society of thyroid Radiology TIRADS, and American thyroid association guidelines, Am. J. Roentgenol. 210 (2018) 1148–1154, https://doi.org/10.2214/AJR.17.18822.

[11] G. Russ, Risk stratification of thyroid nodules on ultrasonography with the French TI-RADS: description and reflections, Ultrasonography 35 (2015) 25–38, https://doi.org/10.14366/usg.15027.

[12] G. Grani, L. Lamartina, V. Ascoli, D. Bosco, F. Nardi, F. D'Ambrosio, A. Rubini, L. Giacomelli, M. Biffoni, S. Filetti, C. Durante, V. Cantisani, Ultrasonography scoring systems can rule out malignancy in cytologically indeterminate thyroid nodules, Endocrine 57 (2017) 256–261, https://doi.org/10.1007/s12020-016-1148-6.

[13] J.H. Yoon, H.J. Moon, E.-K. Kim, J.Y. Kwak, Inadequate cytology in thyroid nodules: should we repeat aspiration or follow-up? Ann. Surg Oncol. 18 (2011) 1282–1289, https://doi.org/10.1245/s10434-011-1605-7.

[14] J. Ophir, I. Céspedes, H. Ponnekanti, Y. Yazdi, X. Li, Elastography: a quantitative method for imaging the elasticity of biological tissues, Ultrason. Imag. 13 (1991) 111–134, https://doi.org/10.1177/016173469101300201.

[15] R.G. Barr, D. Cosgrove, M. Brock, V. Cantisani, J.M. Correas, A.W. Postema, G. Salomon, M. Tsutsumi, H.-X. Xu, C.F. Dietrich, WFUMB guidelines and recommendations on the clinical use of ultrasound elastography: Part 5. Prostate, Ultrasound Med. Biol. 43 (2017) 27–48, https://doi.org/10.1016/j.ultrasmedbio.2016.06.020.

[16] X.-W. Cui, K.-N. Li, A.-J. Yi, B. Wang, Q. Wei, G.-G. Wu, C. Dietrich, Ultrasound elastography, endosc, Ultrasound 11 (2022) 252, https://doi.org/10.4103/EUS-D-21-00151.

[17] F.-J. Dong, M. Li, Y. Jiao, J.F. Xu, Y. Xiong, L. Zhang, H. Luo, Z.-M. Ding, Acoustic Radiation Force Impulse imaging for detecting thyroid nodules: a systematic review and pooled meta-analysis, Med. Ultrason. 17 (2015) 192, https://doi.org/10.11152/mu.2013.2066.172.hyr.

[18] J. Han, F. Li, C. Peng, Y. Huang, Q. Lin, Y. Liu, L. Cao, J. Zhou, Reducing unnecessary biopsy of breast lesions: preliminary results with combination of strain and shear-wave elastography, Ultrasound Med. Biol. 45 (2019) 2317–2327, https://doi.org/10.1016/j.ultrasmedbio.2019.05.014.

[19] V.S. Gress, E.N. Glawion, J. Schmidberger, W. Kratzer, Comparison of liver shear wave elastography measurements using Siemens acuson S3000, GE LOGIQ E9, philips EPIQ7 and Toshiba aplio 500 (software versions 5.0 and 6.0) in healthy volunteers, Ultraschall Med. - Eur. J. Ultrasound. 40 (2019) 504–512, https://doi.org/10.1055/a-0651-0542.

[20] E.K. Yeon, Y.-M. Sohn, M. Seo, E.-J. Kim, Y.-G. Eun, W.S. Park, S.J. Yun, Diagnostic performance of a combination of shear wave elastography and B-mode ultrasonography in differentiating benign from malignant thyroid nodules, Clin. Exp. Otorhinolaryngol. 13 (2020) 186–193, https://doi.org/10.21053/ceo.2019.01235.

[21] X. Li, J. Yu, Z.-Y. Han, H.-Y. Zhai, P. Liang, S.-B. Duan, Diagnostic value of two-dimensional shear wave elastography in papillary thyroid microcarcinoma, OncoTargets Ther. (2016) 1311, https://doi.org/10.2147/OTT.S98583.

[22] L.-J. Liao, H.-W. Chen, W.-L. Hsu, Y.-S. Chen, Comparison of strain elastography, shear wave elastography, and conventional ultrasound in diagnosing thyroid nodules, J. Med. Ultrasound 27 (2019) 26, https://doi.org/10.4103/JMU.JMU_46_18.
[23] F. Zhang, X. Zhao, R. Han, M. Du, P. Li, X. Ji, Comparison of acoustic radiation force impulse imaging and strain elastography in differentiating malignant from benign thyroid nodules: elastography for thyroid nodules, J. Ultrasound Med. 36 (2017) 2533–2543, https://doi.org/10.1002/jum.14302.
[24] J.P. Brito, J.C. Morris, V.M. Montori, Thyroid cancer: zealous imaging has increased detection and treatment of low risk tumours, BMJ 347 (2013), https://doi.org/10.1136/bmj.f4706 f4706–f4706.
[25] T. Kara, F. Ateş, M.S. Durmaz, N. Akyürek, F.G. Durmaz, B. Özbakır, M. Öztürk, Assessment of thyroid gland elasticity with shear-wave elastography in Hashimoto's thyroiditis patients, J. Ultrasound. 23 (2020) 543–551, https://doi.org/10.1007/s40477-020-00437-y.
[26] R.H.C. Filho, F.L. Pereira, W. Iared, Diagnostic accuracy evaluation of two-dimensional shear wave elastography in the differentiation between benign and malignant thyroid nodules: systematic review and meta-analysis, J. Ultrasound Med. 39 (2020) 1729–1741, https://doi.org/10.1002/jum.15271.
[27] W. Li, Y. Wang, J. Wen, L. Zhang, Y. Sun, Diagnostic performance of American College of Radiology TI-RADS: a systematic review and meta-analysis, Am. J. Roentgenol. 216 (2021) 38–47, https://doi.org/10.2214/AJR.19.22691.
[28] G. Bora Makal, A. Aslan, The diagnostic value of the American College of Radiology thyroid imaging reporting and data system classification and shear-wave elastography for the differentiation of thyroid nodules, Ultrasound Med. Biol. 47 (2021) 1227–1234, https://doi.org/10.1016/j.ultrasmedbio.2021.01.023.
[29] W.-B. Zhang, J.-J. Li, X.-Y. Chen, B.-L. He, R.-H. Shen, H. Liu, J. Chen, X.-F. He, SWE combined with ACR TI-RADS categories for malignancy risk stratification of thyroid nodules with indeterminate FNA cytology, Clin. Hemorheol. Microcirc. 76 (2020) 381–390, https://doi.org/10.3233/CH-200893.
[30] X.-Q. Gao, Y. Ma, X.-S. Peng, L.-L. Wang, H.-X. Li, X.-L. Zheng, Y. Liu, Diagnostic performance of C-TIRADS combined with SWE for the diagnosis of thyroid nodules, Front. Endocrinol. 13 (2022), 939303, https://doi.org/10.3389/fendo.2022.939303.
[31] B. Liu, J. Liang, Y. Zheng, X. Xie, G. Huang, L. Zhou, W. Wang, M. Lu, Two-dimensional shear wave elastography as promising diagnostic tool for predicting malignant thyroid nodules: a prospective single-centre experience, Eur. Radiol. 25 (2015) 624–634, https://doi.org/10.1007/s00330-014-3455-8.